Stress field associated with elliptical inclusions in a deforming matrix: Mathematical model and implications for tectonic overpressure in the lithosphere

Author(s):
Moulas, Evangelos; Burg, Jean-Pierre; Podladchikov, Yuri Y.

Publication date:
2014-09-15

Permanent link:
https://doi.org/10.3929/ethz-a-010744277

Originally published in:
Tectonophysics 631, https://doi.org/10.1016/j.tecto.2014.05.004

Funding acknowledgement:
335577 - Interplay between metamorphism and deformation in the Earth's lithosphere (EC)

Stress field associated with elliptical inclusions in a deforming matrix: mathematical model and implications for tectonic overpressure in the lithosphere

Evangelos Moulas*, Jean-Pierre Burg*, Yuri Podladchikov**

*Department of Earth Sciences, ETH-Zurich, Switzerland

**Institute of Earth Sciences, ISTE, University of Lausanne, Switzerland

ABSTRACT

Shear zones and competent layers and boudins represent viscosity heterogeneities within the rock mass. Differences in viscosity impel differences in strain rates between the background material and the heterogeneities. In this work, we represent the viscosity heterogeneities as elliptical inclusions. We use the Kolosov-Muskhelishvili equations for the incompressible viscous flow problem in and around elliptical inclusions. Systematic investigation of the stress equilibrium at the matrix-inclusion interface shows that the mean stress, equivalent to the total pressure, is not continuous across viscosity boundaries. The results predict that pressure and stress perturbations depend strongly on the orientation of the elliptical heterogeneity with respect to the far-field stresses. A viscosity ratio of 10 between the inclusion and the surrounding material is sufficient to produce pressure discontinuities approximately equal to the magnitude of the effective shear stress of the strongest rock under the considered physical conditions. Comparison of the analytical solutions with thermo-mechanical models confirms pressure incongruity and suggests that dynamic parameters such as pressure and effective shear stress vary spatially and temporally within deforming, two-viscosity rock systems. As a corollary, the dependence of metamorphic phase equilibria on thermodynamic pressure implies that shear zones, taken as weak inclusions, and boudins, taken as hard inclusions, may record non-lithostatic pressure during deformation.

INTRODUCTION

The advent of geothermobarometry from metamorphic phase equilibria (e.g. Perchuk, 1991) has led to the quantitative determination of pressure and temperature (*P*-*T*) histories of metamorphic rocks. As a first approximation the depth-of-burial of metamorphic rocks is estimated from the Archimede's formula. This formula is derived from the stress balance of static fluids under the influence of gravity and relates pressure with depth via:

$$P_{lith} = \rho g h \qquad (1)$$

where P_{lith} is the lithostatic pressure, ρ is the density of the considered material, g is the acceleration of gravity and h is the height of the hydrostatic (lithostatic for rocks) column (depth). Stresses that develop during deformation can affect the value of pressure. In that case, pressure deviates from the lithostatic pressure state in a positive (over-pressure) or negative (under-pressure) manner.

Several studies have already argued that the pressure recorded by the metamorphic minerals could significantly differ from the lithostatic pressure (e.g. Clark, 1961; Jamieson 1963; Petrini and Podladchikov, 2000; Mancktelow, 2008). This pressure deviation is directly related to the mechanical state of the deforming rocks. This long-existing concept has been repeatedly disputed. Considering the mechanical properties of rocks, several studies have suggested that the magnitude of pressure deviation from the lithostatic value is small, almost insignificant because rocks are weak and the differential stress that controls natural deformation is low (Brace et al., 1970; Burov et al., 2001; Jolivet et al., 2003). Actually, Brace et al. (1970) reported GPa-level differential stresses ranging from 0.2 to ca 1.1 GPa from the Franciscan rocks; yet, they rejected their experimental result on the assumption that, under geological conditions, the presence of fluids, the low strain rates and the high temperatures reduce the strength of rocks. There are reasons to believe that this may not be the case. Recent experiments suggest that GPa-level of stresses can be supported by the weakest high-pressure phase (omphacitic pyroxene) when extrapolated to geological conditions (Moghadam et al., 2010). In addition recent numerical models (Schmalholz and Podladchikov, 2013) suggest that low viscosity zones may develop significant over/under pressure despite their low effective shear stress.

Finite strain recorded in viscously deformed rocks does not suffice to provide information regarding the magnitude and orientation of stress which occurred during deformation. Without this information,

estimates of dynamic variables, such as pressure and effective shear stress, cannot be made. In order to investigate the correlation between effective shear stress and mean stress during viscous deformation, we employ the Kolosov-Muskhelishvili analytical solution for slow, incompressible viscous flow (Kolosov, 1909; Muskhelishvili, 1953). We used the analytical solution of Schmid and Podladchikov, (2003) and applied this solution to viscous heterogeneities under various geometrical configurations. Viscous heterogeneities are treated as elliptical inclusions. Results are compared with those of thermo-mechanical models with more complex temperature-dependent rheologies (Schmalholz and Podladchikov, 2013). The comparison allows verifying that the classical analytical solution is relevant to geological applications and shows that pronounced pressure departures from lithostatic can develop due to viscosity heterogeneities. This work indicates that (1) the viscosity contrast and aspect ratio control the magnitude of the pressure difference and (2) the inclination of the inclusion with respect to the bulk compression direction controls the spatial distribution of pressure. Both weak and strong inclusions can develop large pressure variations depending on geometrical and rheological factors.

These analytical results applied to geological cases such as low-viscosity shear zones and highly viscous boudins suggest that the viscosity heterogeneities they represent in nature cause pressure deviations from the lithostatic value. The pressure differences can reach the order of GPa when the strength of the rocks is taken into account. Hence, it is concluded that the pressure recorded by syn-deformation metamorphic parageneses may be misleading for depth estimates.

TERMINOLOGY: EFFECTIVE SHEAR STRESS, MEAN STRESS, PRESSURE AND THERMODYNAMIC PRESSURE

In this work we estimate dynamic parameters such as the effective shear stress and pressure. The effective or maximum shear stress (τ) is (Nadai, 1950, p. 95):

$$\tau = \sqrt{\left(\frac{\left(\sigma_{xx}\right)_{tot} - \left(\sigma_{yy}\right)_{tot}}{2} \right)^2 + \left(\sigma_{xy}\right)_{tot}^{\,2}} \qquad (2)$$

where $(\sigma_{ij})_{tot}$ are components of the total stress tensor; stress components $(\sigma_{ij})_{tot}$ are taken as positive in extension to follow classical convention in continuum mechanics, knowing that a sign inversion does not affect the essence of results. The differential stress (σ_d) is the difference between the largest and smallest principal stresses (σ_1 and σ_3 where $\sigma_1 > \sigma_2 > \sigma_3$) and the relation between σ_d and τ is (e.g.

Nadai, 1950, p. 95):

$$\sigma_d = 2\tau \qquad (3)$$

Mean stress is synonymous to pressure. Considering viscous flow in two dimensions the total pressure equals (Timoshenko and Goodier, 1951):

$$P_{tot} = \frac{-\left(\sigma_{xx}\right)_{tot} + \left(\sigma_{yy}\right)_{tot}}{2} \qquad (4)$$

The total pressure is positive in compression. When deforming geomaterials are considered, the total pressure can be decomposed into a lithostatic (from the influence of gravity) and a dynamic (tectonic over/under pressure) component.

Different views have been expressed on which pressure is actually recorded by metamorphic phase equilibria (i.e. the thermodynamic pressure). Fluid pressure, mean stress and local normal stresses at the surface of minerals have been suggested to be the controlling factors of thermodynamic equilibrium (e.g. Paterson, 1973; Dahlen, 1992; Llana-Fúnez et al., 2012). These three values are not expected to deviate significantly from the lithostatic pressure where differential stress is low. On the other hand, if the differential stress is large, then fluid pressure, mean stress, and local normal stress may range so widely that they can affect the thermodynamic phase relations (e.g. Hirth and Tullis, 1994). Quantifying the potential variations in pressure can therefore test the validity of the pressure to depth translation which is important for geodynamic reconstructions.

METHODS

Muskhelishivili's method (Muskhelishvili, 1953) utilizes complex variables to solve the bi-harmonic equations for plane-strain or plane-stress elasticity problems. In geology plane strain is usually considered as a reasonable approximation to problems where most of the displacements occur in a single plane. Mathematically, the all-viscous solution is identical to the all-elastic solution (Goodier, 1936). The main difference between the two solutions is that the elastic shear modulus is replaced by viscosity and elastic strain is replaced by strain rate. For the all-viscous deformation, we use the Kolosov-Muskhelishvili equations as implemented by Schmid and Podladchikov (2003). We vary geometrical parameters such as the inclination (α) and the aspect ratio (κ) of a viscous elliptical

inclusion embedded in a viscous matrix. We consider different viscosity ratios between the inclusion and the matrix (μ^i/μ^m). The angle between the principle axis of the ellipse and direction of compression is denoted via α (Fig. 1). All the previous parameters are sufficient to calculate the mean stress (P), the effective shear stress (τ) and the local orientation of the maximum compressive stress (ω) of the viscous problem. The angle ω is the inclination of this stress with respect to the far-field maximum compressive stress (which is horizontal; Fig.1). θ is the variable angle between the normal to the inclusion-matrix interface and the horizontal. This angle is required to parametrize the matrix effective shear stress and pressure at the interface on the matrix side. Superscripts i and m are used to discriminate between inclusion and matrix, respectively. The subscript ffs will denote far-field conditions (e.g. P_{ffs} stands for far-field mean stress).

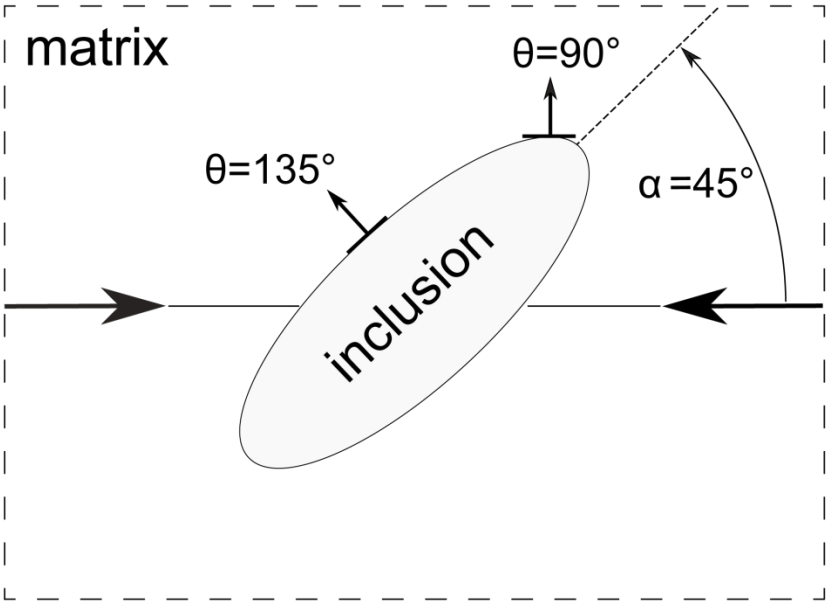

Fig. 1. Sketch illustrating the angle convention used in this study. Angles are measured counter-clockwise from the horizontal far-field-compressive stress (arrows).

ANALYTICAL SOLUTION AND COMPARISON WITH NUMERICAL RESULTS

Reducing the number of controlling parameters

The analytical solution gives mathematical expressions for homogenous stress and pressure fields in a viscous medium without inclusion and for stress and pressure perturbations due to an elliptical inclusion in its viscous matrix. The two stress states are additive and the analytical solutions for the

perturbations are insensitive to the mechanism responsible for the background homogeneous state (e.g. lithostatic load). Perturbation of the pressure for matrix or inclusion is formally equal to:

$$P = P_{tot} - P_{ffs} \qquad (5)$$

Similarly, stress components are:

$$\sigma_{xx} = \left(\sigma_{xx}\right)_{tot} - P_{ffs} \qquad (6)$$

$$\sigma_{yy} = \left(\sigma_{yy}\right)_{tot} - P_{ffs}$$

but

$$\sigma_{xy} = \left(\sigma_{xy}\right)_{tot}$$

The far-field boundary condition is a homogeneous stress state with zero mean stress. The choice of the principal stress directions as coordinate system eliminates the shear stress components and leaves τ_{ffs} as the only parameter needed to identify the stress field. The far-field stress tensor is:

$$\sigma_{ffs} = \begin{pmatrix} -\tau_{ffs} & 0 \\ 0 & \tau_{ffs} \end{pmatrix} \qquad (7)$$

The pressure and stress perturbations are linearly proportional to the magnitude of τ_{ffs}. Therefore, we normalize the solutions to τ_{ffs}. The total pressure can be recovered as:

$$P_{tot} = \frac{P}{\tau_{ffs}} \tau_{ffs} + P_{ffs} \qquad (8)$$

The solution for a completely arbitrary stress state can be obtained by adding a value of the far field mean stress to the analytical solution for the stress perturbation and by rotating the coordinate system.

Analytical solution and Mohr circle representation

The calculations were performed for a weak (less viscous; Fig. 2) and a strong (more viscous; Fig. 3) inclusion, each at four orientations. Results are displayed as color maps of the pressure field (Figs. 2 and 3). Stress Mohr circles document the pressure (P: center of the Mohr circle) and the effective shear

stress (τ: radius of the Mohr circle) supported by the inclusion and the surrounding matrix. The far-field effective shear stress to which all calculations are normalized (τ_{ffs}) becomes in this representation a circle with unit radius centered on the origin. The convention followed for the Mohr-circle representation is that compressive stress is positive (e.g. Means, 1976).

The usage of Mohr circles illustrates how and why pressure differentials develop. Mohr circles of each material have different radius because materials have different viscosity, therefore different effective shear stress (τ). The intersection of the related Mohr circles defines the plane of stress equilibrium between the two considered materials. In that case, the centers of the Mohr circles do not coincide (e.g. Fig. 3b), which pictures the difference in mean stress (and therefore pressure, P) in each material.

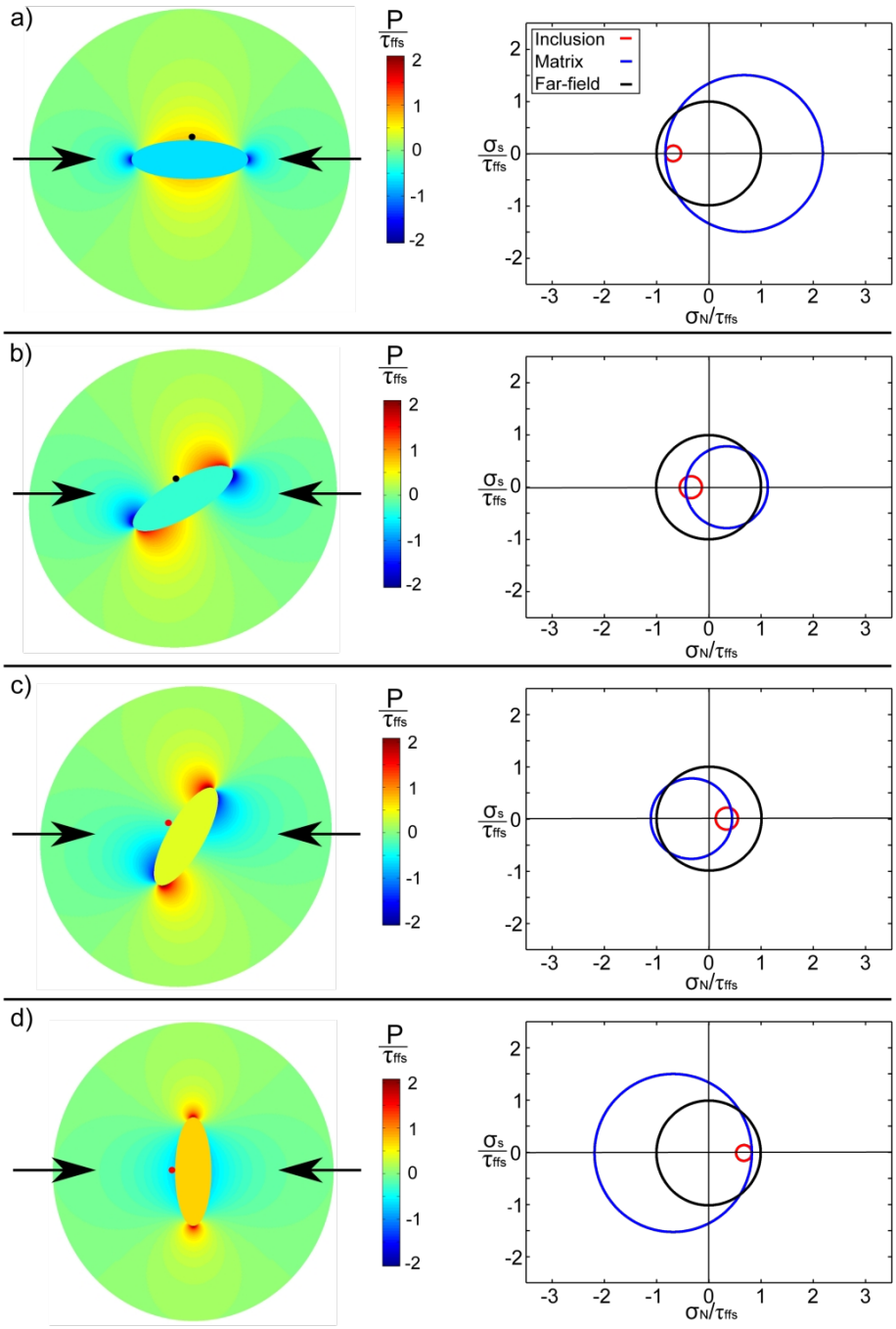

Fig. 2. Stress distribution in and around a weak viscous inclusion in a viscous matrix. Left panes show pressure of solutions with orientations (α) at 0° (a), at 30° (b), at 60° (c) and at 90° (d) from the compressive far-field stress (converging arrows). Parameters are: κ=3, and μ^i/μ^m = 0.1. Mohr circles computed using the stress defined at the location of the solid dot identified on the interface between the inclusion and the matrix. The horizontal axis in the Mohr diagrams represents the normalized normal stress (σ_N) and the vertical axis represents the normalized shear stress (σ_s) that can develop on any arbitrary plane passing from the considered material points.

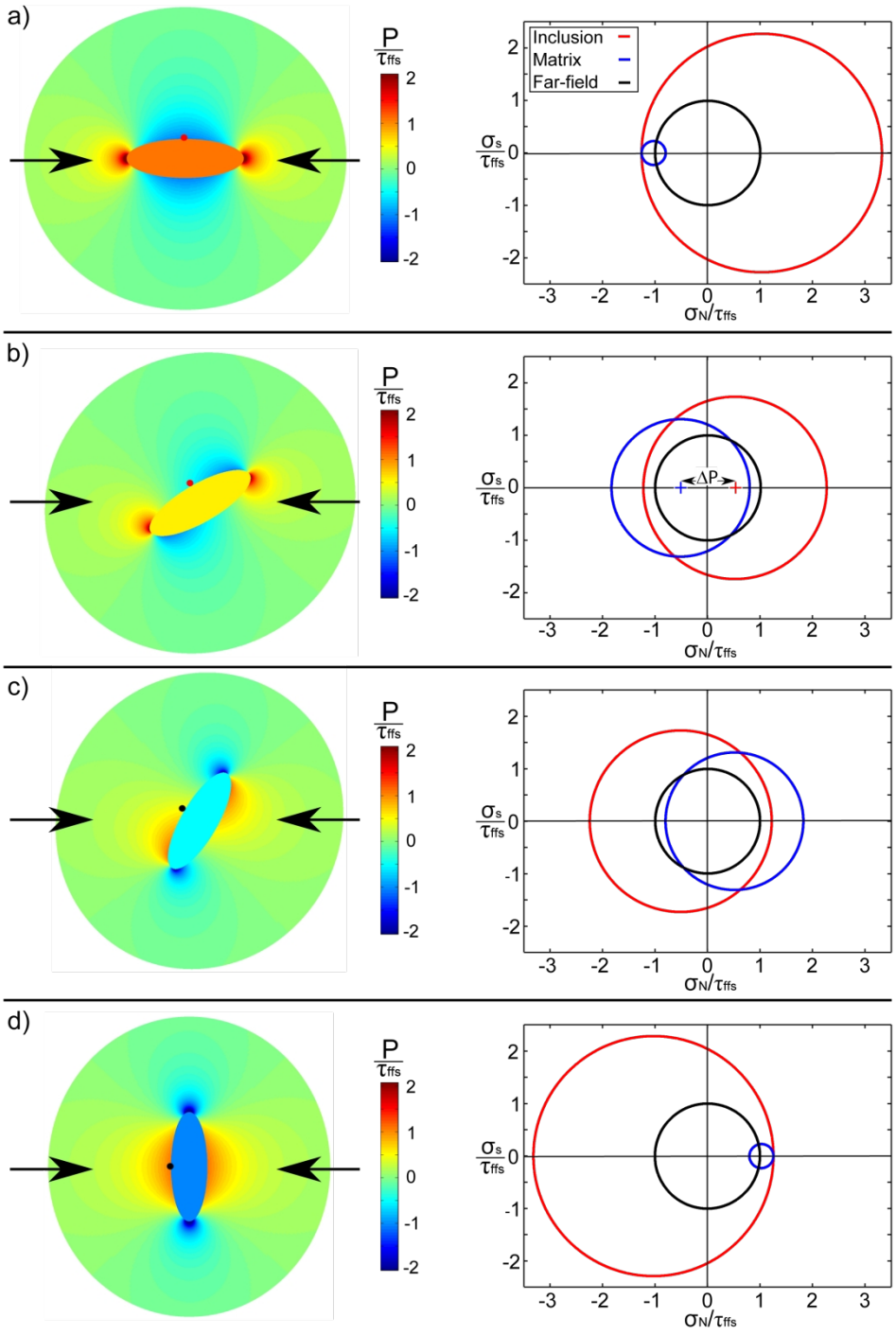

Fig. 3. Same as Fig. 2 but for a strong viscous inclusion ($\mu^i/\mu^m = 10$).

Main results

Taking the inclusion orientation (α) as an independent parameter, the distinction between pure or

simple shear is redundant. It can be expressed through a mere rotation by 45º of the coordinate system (c.f. Schmid and Podladchikov, 2003). The results show that the dynamic variables (P, τ, ω) are constant within the viscous inclusion but vary in the matrix (Figs. 2 and 3). The pressure P inside a weak (less viscous) inclusion is positive for 45º<α<90º and becomes negative for 0º <α<45º (Fig. 2). Pressure P has the opposite behavior if a strong viscous inclusion is considered (Fig. 3).

Consistency test

We compare the analytical results with results from the numerical simulations of Schmalholz and Podladchikov, (2013). This comparison tests the relevance of our results for more complex, temperature-dependent nonlinear rheology and for weak zones that are imperfect elliptical inclusions (Figs. 4, 5). Schmalholz and Podladchikov, (2013) obtained a self-localizing, finite shear zone inclined at 60º (α=120° based on the convention followed here) from the bulk shortening and propagating from a small viscous, circular seed. They calculated similar dynamic parameters as in this work: tectonic overpressure, effective shear stress and maximum-compressive-stress orientation at any point of their model.

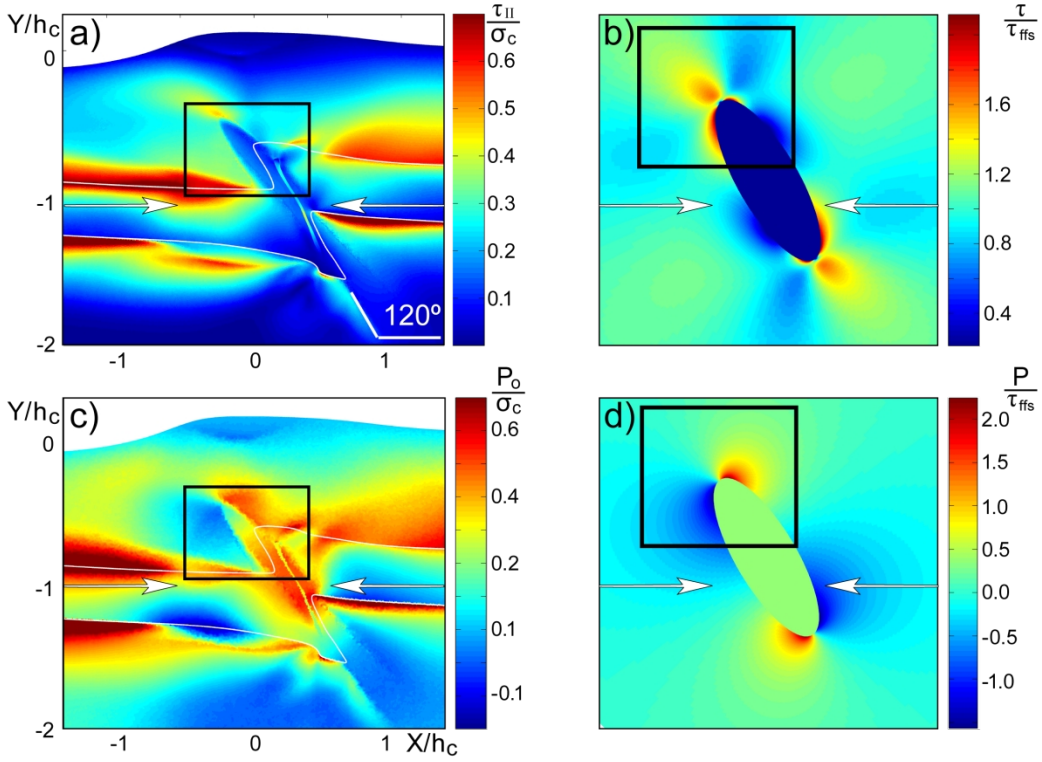

Fig. 4. Second stress invariant (a) and deviation from lithostatic pressure (c) during lithospheric shortening after Schmalholz and Podladchikov (2013). X/h_c and Y/h_c represent the width and the height of the model normalized to the initial thickness of the crust (h_c). Comparison of similar dynamic parameters from our analytical solutions (b, d). Note that in two dimensions the second stress invariant (τ_{II}) and the effective shear stress (τ) are equal. Parameters in b and d are $\kappa=3$, $\alpha=120°$, $\mu^i/\mu^m = 0.1$.

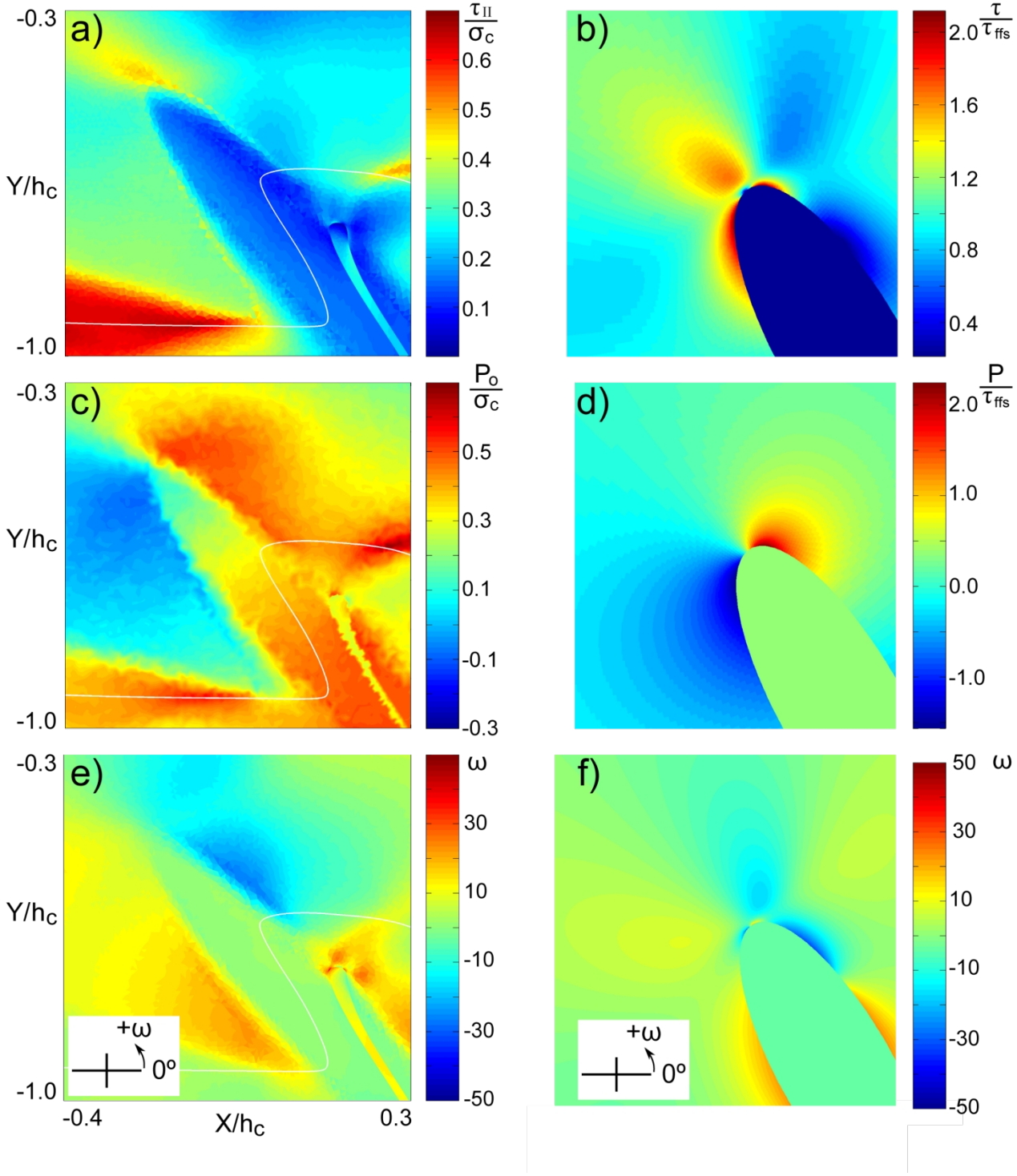

Fig. 5. Detail framed in Fig. 4.a, b, c, d same as in Fig. 4. e) Maximum-compressive-stress orientation (ω) from the numerical results of Schmalholz and Podladchikov (2013). f) Maximum-compressive-stress orientation (ω) from the analytical solution (κ=3, α=120°, μ^i/μ^m = 0.1).

Schmalholz and Podladchikov (2013) calculated the second stress invariant τ_{II}. Our analytical solution calculates the effective shear stress (τ, Eq. 2). In two dimensions, these two values and formulation are mathematically identical. Schmalholz and Podladchikov (2013) used P_o to describe the deviation from the lithostatic pressure.

$$P_o = P_{tot} - P_{lith} \qquad (9)$$

This formulation has the caveat that the far-field mean stress P_{ffs}, which we use (Eq.5), may not be equal to the lithostatic pressure P_{lith}. Moreover, Schmalholz and Podladchikov normalized all pressure and stresses to the pressure at the Moho, σ_c, whereas we normalized to τ_{ffs}. Owing to these different scaling factors, we focus on similarities between P and P_o patterns but not on the magnitudes of these pressures. This focus is also valid for our calculated τ and the τ_{II} of Schmalholz and Podladchikov, (2013). Comparing a shear zone to a weak, elongated inclusion, our analytical solution reproduces remarkably well their patterns of effective shear stress (τ, Fig. 4 a and b) and tectonic over/under pressure (P_o and P, Fig. 4 c and d).

The angle ω (Fig. 5e and f) displays the same consistency. An aspect ratio of three (κ=3) was chosen for our analytical solution. This value was estimated as a lower bound for the shear zone (low effective shear stress zone Fig. 5a) of the numerical results. Higher aspect ratios would amplify the stress and pressure magnitudes but would not significantly alter their distribution, as shown in the following section. This application demonstrates the applicability of our results, even for more complex rheological systems.

SYSTEMATIC INVESTIGATIONS

Inclusion behaviour

A striking peculiarity of the analytical solution is the constant pressure (P) and effective shear stress (τ) within the inclusion. Accordingly, the inclusion behaviour can be described by a single value for effective shear stress (τ^i), pressure (P^i) and maximum-compressive-stress orientation (ω^i).

The pressure inside the viscous inclusion is given by the formula:

$$\frac{P^i}{\tau_{ffs}} = \frac{\left(\frac{\mu^i}{\mu^m} - 1\right)\left(\kappa^2 - 1\right)}{2\left(\frac{\mu^i}{\mu^m}\right)\kappa + \kappa^2 + 1}\cos\left(2\alpha\right) \qquad (10)$$

that shows the dependence of the sign of the pressure perturbation on the orientation of the viscous elliptical inclusion.

We carried out systematic calculations in order to investigate how P^i, τ^i and ω^i depend on the inclusion inclination and viscosity contrast (Fig. 6). P and τ within the inclusion follow a periodic variation in accordance with the inclusion orientation. Pressure and effective shear stress have different periodicities so that their magnitude minima and maxima do not coincide. The maximum angle ω is < 10º, which suggests small stress refraction into the inclusion.

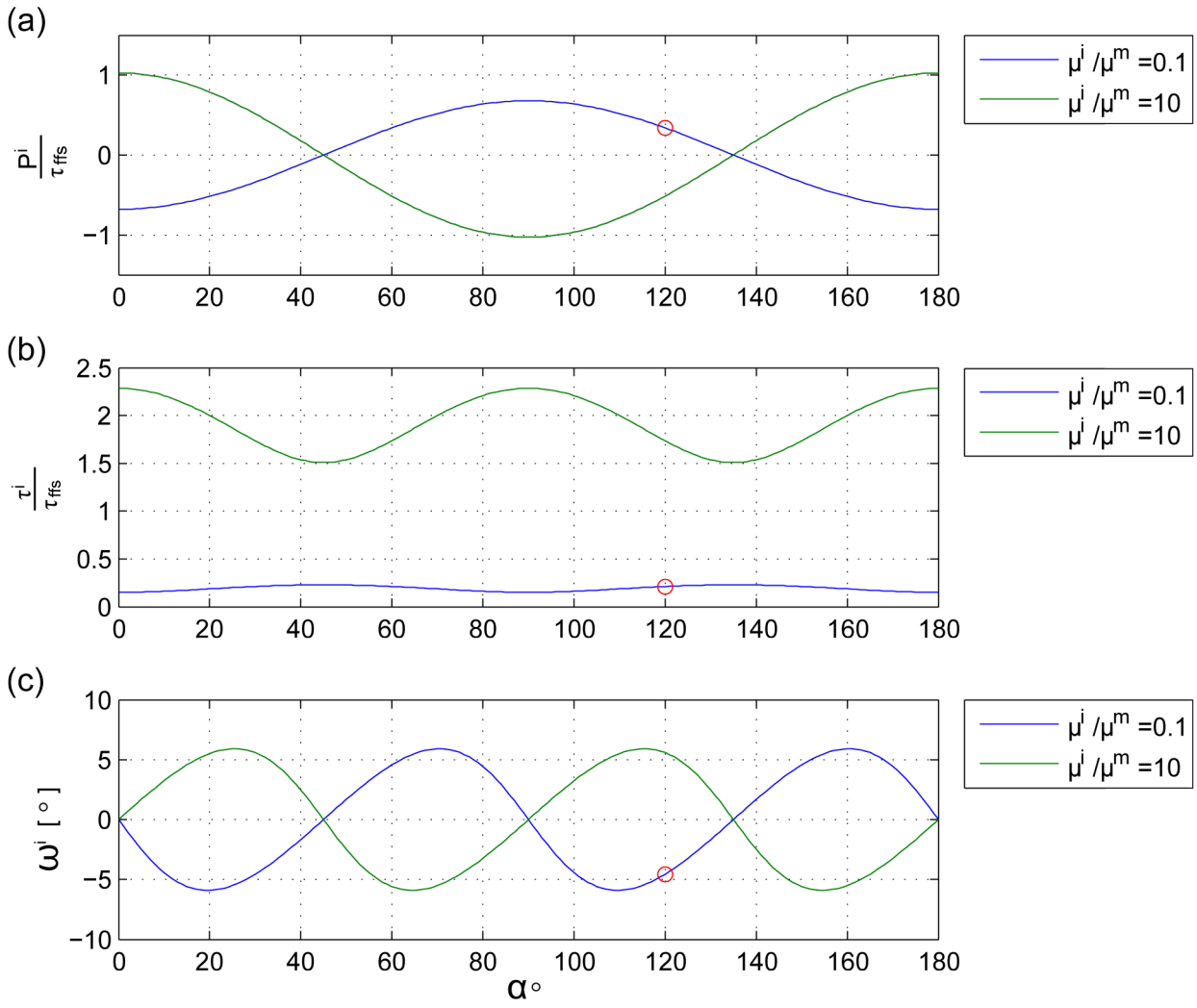

Fig. 6. a) Variation of pressure (P^i/τ_{ffs}), b) maximum shear stress (τ^i/τ_{ffs}) and c) maximum-compressive-stress orientation (ω^i) within the inclusion (κ=3) as a function of orientation (α) and viscosity ratio (μ^i/μ^m). The red circle indicates the parameters of the inclusion shown in Figs. 5b, d (κ=3, α=120°, μ^i/μ^m = 0.1).

The p-q diagram (Lambe and Whitman, 1968) allows representing the states of stress of the inclusion. This diagram plots the pressure (mean stress; center of the Mohr circle) P versus the effective shear stress (radius of Mohr circle) q (equal to τ). The advantage of the p-q diagram is that all the stress states are described for all α. The p-q diagram was calculated for six orders of magnitude in viscosity ratios. The resulting effective shear stress can vary by several orders of magnitude. For convenience, we modified the p-q diagram by normalizing the local effective shear stress (τ^i) to the maximal effective shear stress (τ^i_{max}) of each case (Fig. 7). The plot shows that pressure P in a strong inclusion is proportional to the effective shear stress τ. Conversely, pressure in a weak inclusion is inversely related

to the effective shear stress τ.

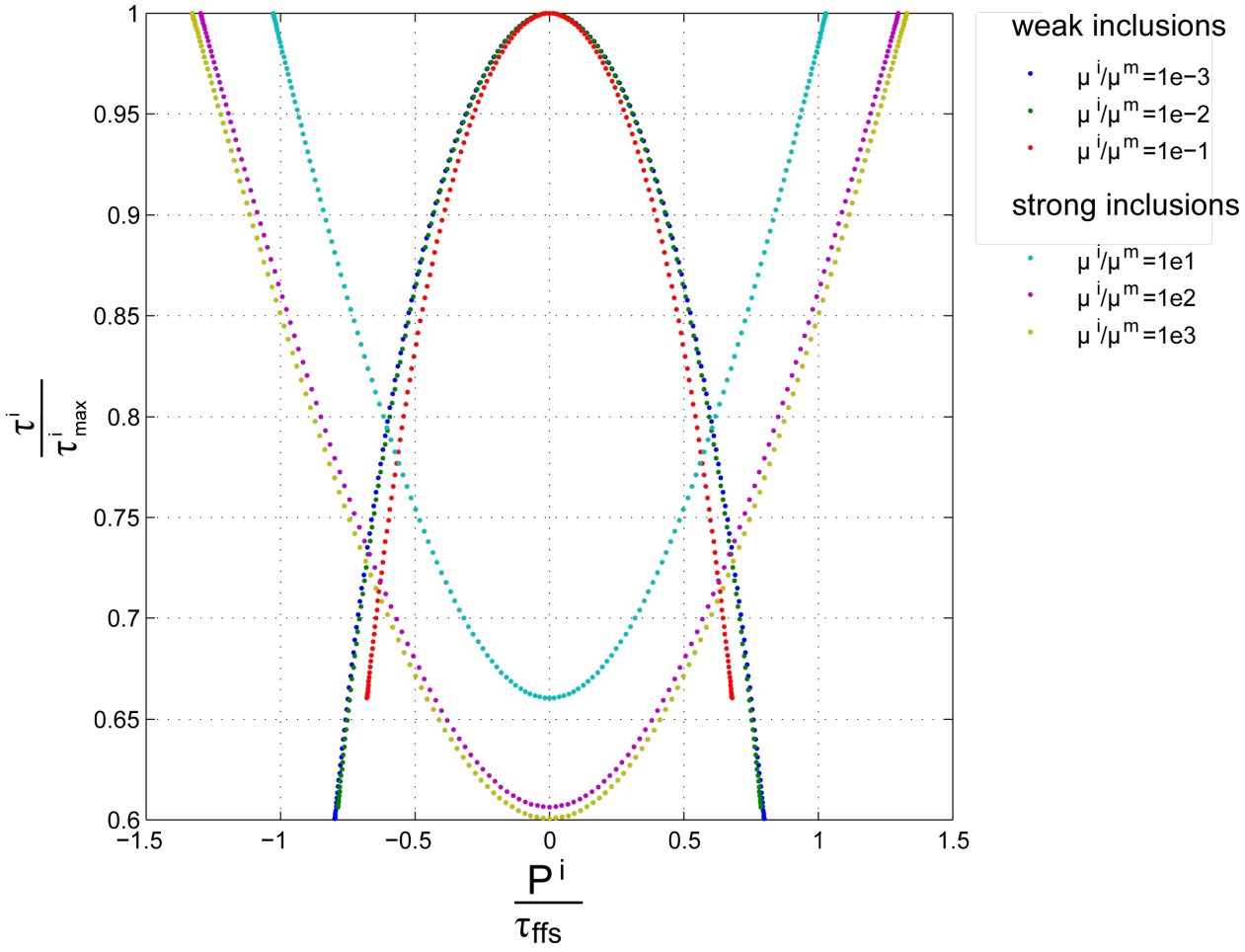

Fig. 7. Modified p-q diagram describing stress states in viscous inclusions (κ=3) for different viscosity ratios (μ^i/μ^m).

Although Fig. 6 shows that P^i, τ^i and ω^i vary periodically as a function of the inclusion orientation (α), the absolute magnitude of the periodic variations is controlled by the aspect ratio of the inclusion (κ) and the viscosity ratio between the inclusion and the matrix (μ^i/μ^m). Therefore, for different inclusion inclinations (α) the amplitude (P^i_{max}/τ_{ffs}, τ^i_{max}/τ_{ffs}, ω^i_{max}) of the sinusoidal variations (e.g. Fig. 6) was calculated (Fig. 8). Generally, higher viscosity ratios and higher aspect ratios both amplify P^i_{max}, τ^i_{max} and ω^i_{max}.

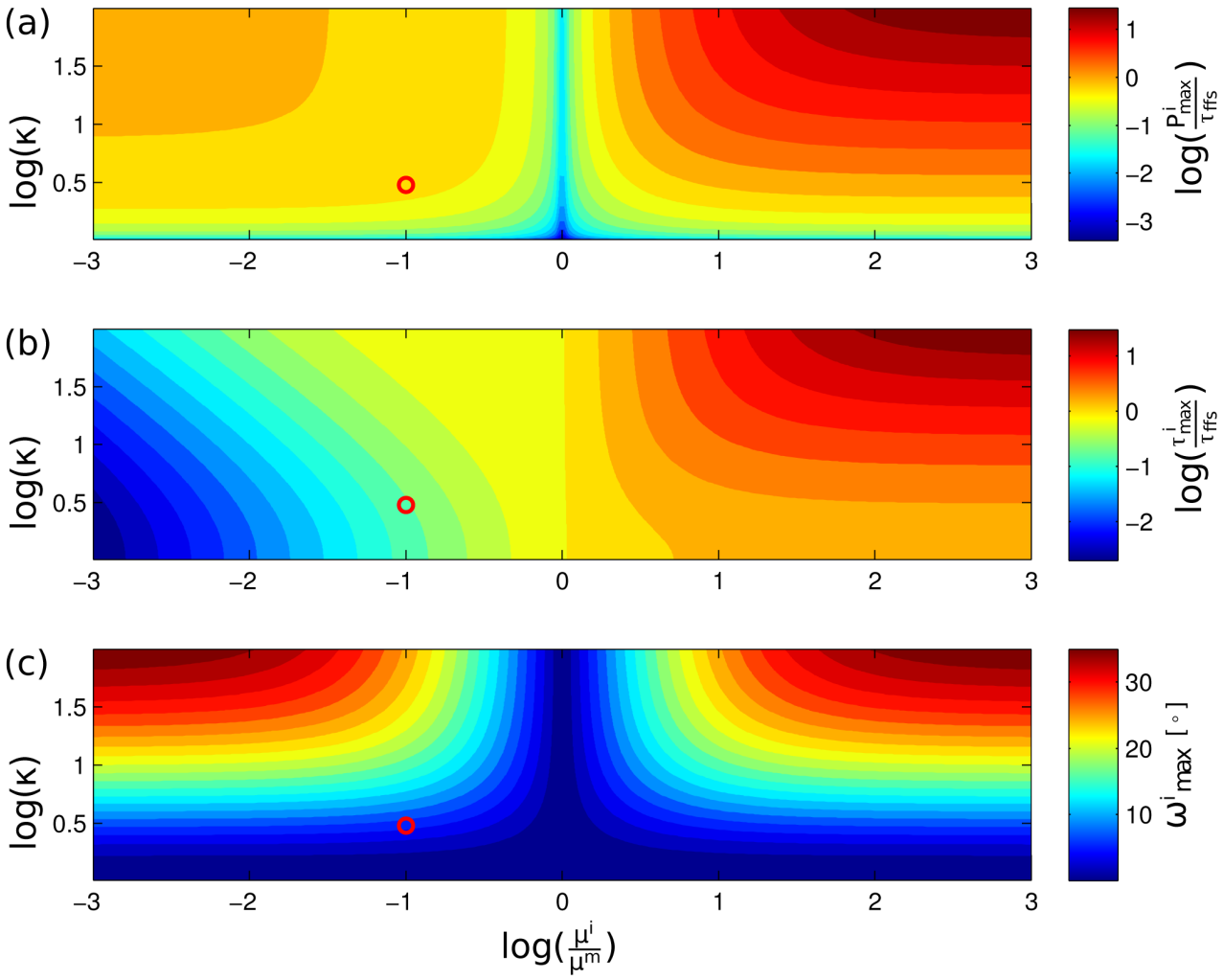

Fig. 8. Maximal magnitudes for all (α) (Fig. 6) of a) normalized Pressure (P^i/τ_{ffs}), b) normalized-effective shear-stress (τ^i/τ_{ffs}) and c) maximum-compressive stress orientation (ω^i) within the inclusion as a function of aspect ratio (κ) and viscosity ratio (μ^i/μ^m). The red circle indicates the inclusion of Fig. 4b, d.

Matrix behaviour

We use the direction of the vector normal to the interface (θ, Fig. 1) to describe how pressure (P^m), effective shear stress (τ^m) and local-compressive-stress orientation (ω^m) vary around the inclusion-matrix interface. The three dynamic parameters show again a periodic behavior for any given θ, (Fig. 9). Although ω^m is in general a periodic function, we see that for this inclusion orientation (α=120º) and for the specific aspect ratio (κ=3), ω^m becomes asymmetric. The asymmetric shape of the ω^m curve is due to the stress distribution induced by the aspect ratio (κ). Any deviation in shape from a circular inclusion (κ≠1) will cause sharp changes in the dynamic parameters (P^m, τ^m and ω^m) due to the

asymmetry that develops.

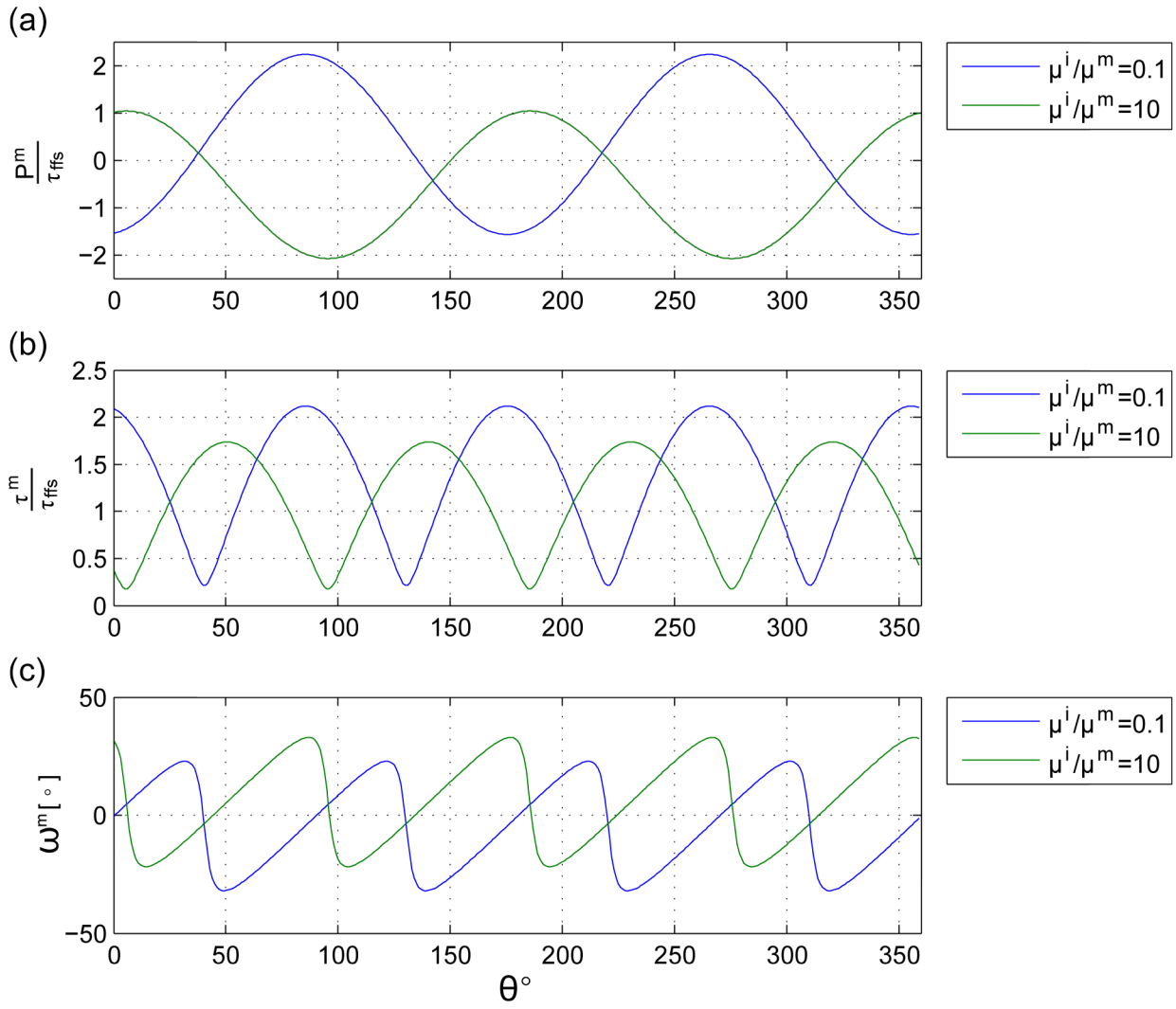

Fig. 9. a) Variation of matrix pressure (P^m/τ_{ffs}), b) effective shear stress (τ^m/τ_{ffs}) and c) maximum-compressive-stress orientation (ω^m) around the inclusion shown in Figs. 4b,d as a function of the normal orientation (θ) and viscosity ratio (μ^i/μ^m). (κ=3, α=120°).

We plotted the data from these sinusoidal variations in function of any inclusion orientation (α) for the six orders of magnitude variations of viscosity ratios considered in Figs. 7 and 8. The resulting diagram (Fig. 10) integrates several variables. For example, for α=120° (black bar in Fig. 10), all possible stress-pressure pairs delineate a vertical bar that has a background colour for the effective shear stress (right-side ordinate in Fig. 10), and a pressure value (left ordinate of Fig. 10). In order to

deduce the general trends of pressure P^m and effective shear stress (τ^m), we use the inclusion pressure (P^i) as a reference and we normalize it using the maximum values of P^m_{max} and τ^m_{max} in the matrix, the normalized pressure difference between inclusion and matrix is given by:

$$\delta P = \frac{P^m - P^i}{P^m_{max} - P^i} \qquad (11)$$

In this equation, the dependence of P and τ on the magnitude of the viscosity ratio is eliminated because the pressure values in the matrix are compared to the pressure values of the inclusion for each case. Therefore any difference between inclusion and matrix pressure caused by the viscosity contrast becomes insignificant.

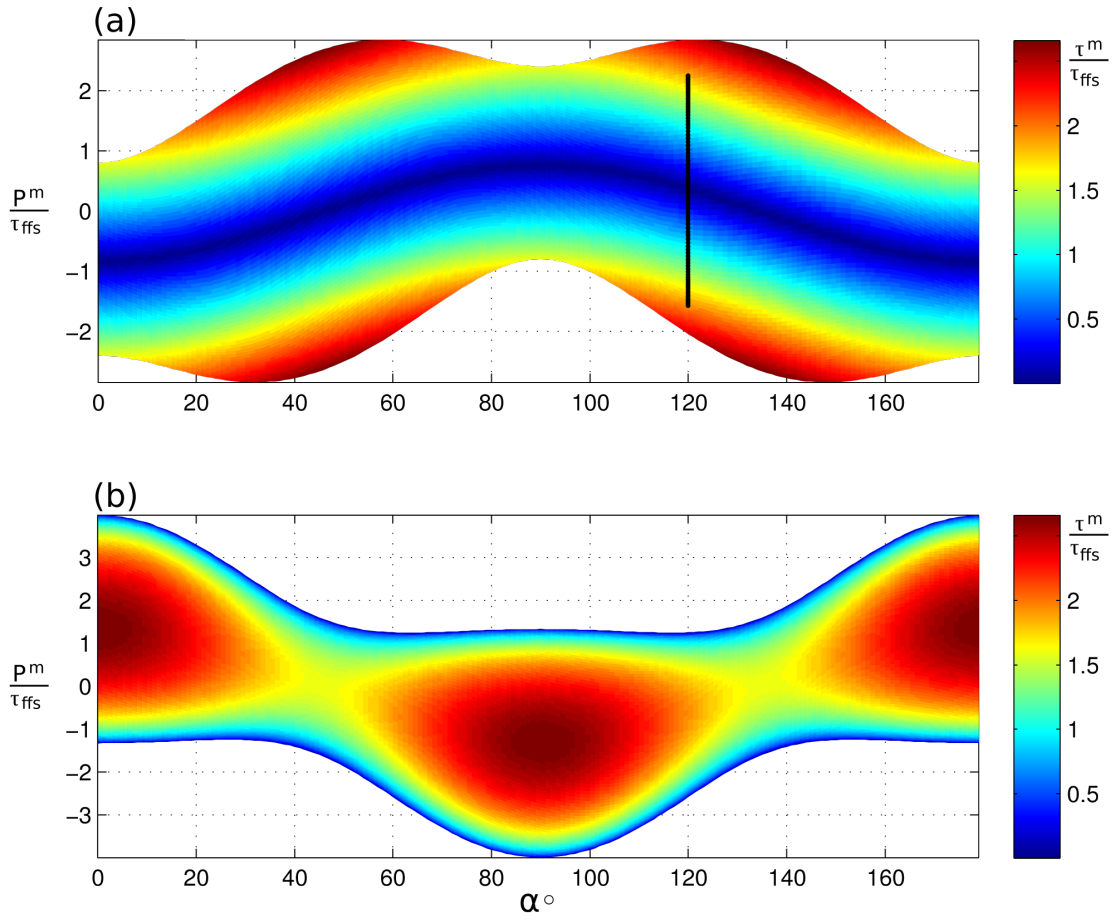

Fig. 10. Values of normalized effective shear stress (τ^m/τ_{ffs}) and normalized pressure (P^m/τ_{ffs}) around the inclusion for different inclusion orientations (α). a) weak inclusion with κ=3, $\mu^i/\mu^m = 10^{-3}$ b) strong inclusion with κ=3, $\mu^i/\mu^m = 10^3$. The bar in (a) corresponds to the stress-states τ (colour scale) around the inclusion of Figs. 5b, d

(κ=3, α=120°, $\mu^i/\mu^m = 10^{-1}$).

All results concerning the matrix are collapsed into two linear relationships (Fig. 11). For a matrix stronger than the inclusion, the pressure difference is proportional to the matrix effective shear stress whereas a matrix weaker than the inclusion follows the equation of a circle (Fig. 11):

$$\delta P = \sqrt{1 - \left(\frac{\tau^m}{\tau^m_{max}} \right)^2} \qquad (12)$$

In other words and in agreement with the previous results, a weak matrix will develop the highest pressure difference from the inclusion when its effective shear stress is the lowest. The magnitudes of pressure and effective shear stress perturbations depend on the aspect ratio of the viscous inclusion and its viscosity contrast with its matrix.

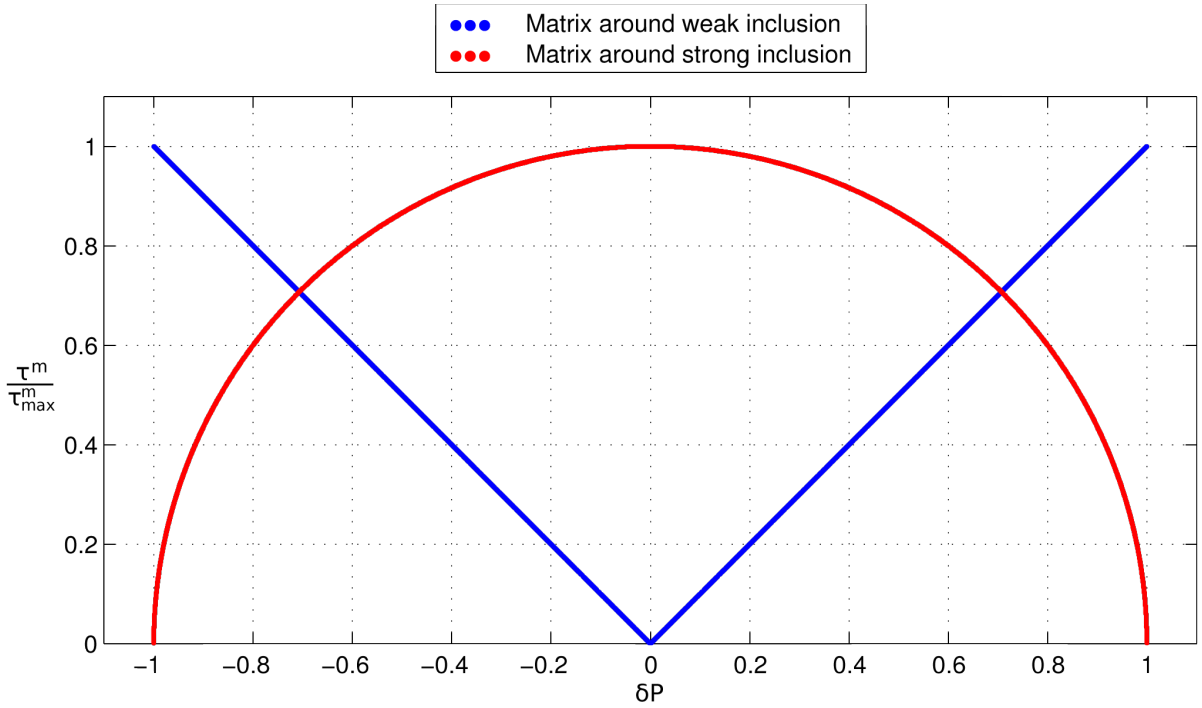

Fig. 11. Normalized difference between pressure in inclusion and pressure in the matrix (δP, Eq. 11) versus the effective shear stress τ^m (normalized over its maximal value τmmax) around an elliptical inclusion. Data from Fig. 10.

In a similar way to the inclusion behavior (Fig. 6), P, τ and ω for the matrix, vary periodically as a function of the inclusion inclination (α). The absolute magnitude of the periodic variations P^{m}_{max}/τ_{ffs}, $\tau^{m}_{max}/\tau_{ffs}$, and ω^{m}_{max} depends on the viscosity ratio between the inclusion and the matrix and on the aspect ratio (κ). Consequently, for different inclusion orientations (α), the amplitude (P^{m}_{max}/τ_{ffs}, $\tau^{m}_{max}/\tau_{ffs}$, and ω^{m}_{max}) of the periodic variations (e.g. Fig. 9) was calculated (Fig. 12). The results suggest that the aspect ratio of the inclusion (κ) and the viscosity ratio between the inclusion and the matrix (μ^{i}/μ^{m}) both amplify P^{m}_{max}/τ_{ffs}, $\tau^{m}_{max}/\tau_{ffs}$, and ω^{m}_{max}.

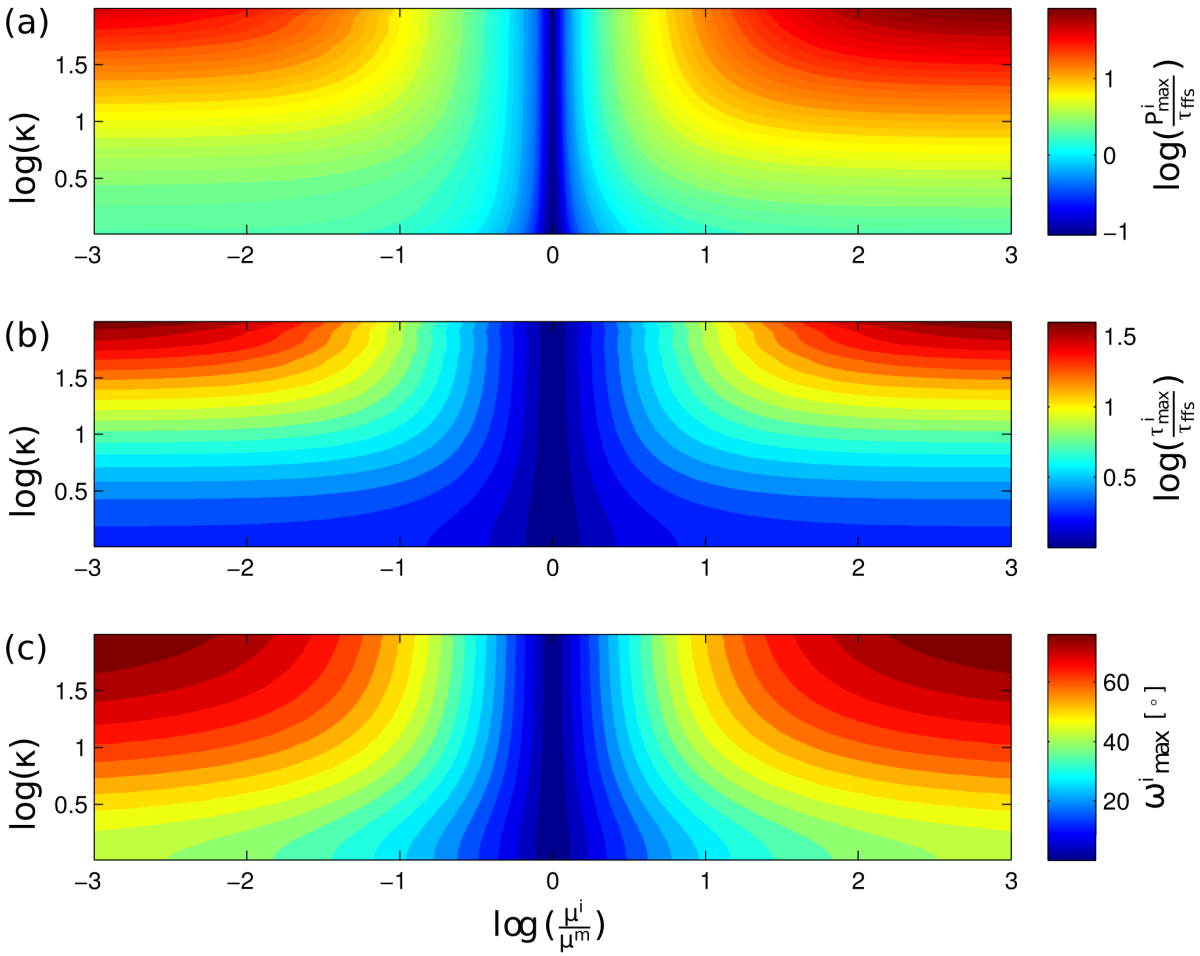

Fig. 12. Maximal magnitudes for all α (Fig. 10) of a) normalized pressure (P^{m}_{max}/τ_{ffs},), b) normalized-effective shear stress ($\tau^{m}_{max}/\tau_{ffs}$,) and c) maximum-compressive stress orientation (ω_{max}) around the inclusion as a function of aspect ratio (κ) and viscosity ratio (μ^{i}/μ^{m}).

APPLICATIONS TO SHEAR ZONES AND BOUDINS

The analytical solution developed in this work has implications for any geological heterogeneity where there is a contrast in viscosity. We consider the applications of our findings to shear zones, which we regard as weak inclusions with high aspect ratio, and boudins, which we regard as strong inclusions.

Shear zones

The systematic study of localized deformation started in the beginning of the 20th century when Inglis (1913) demonstrated that stress drastically concentrates around edges and sharp corners. The quantification of stresses around cracks and holes (Inglis 1913; Griffith, 1921; Irwin, 1957) led to conceptual models in which cracks and discontinuities are treated as elliptic voids of various aspect ratios. In geology, concepts of fracture mechanics have been used to describe fracture propagation, stress nucleation and fault growth (e.g. Pollard and Fletcher, 2005). The underlying assumption is that elliptical inclusions are treated as voids with negligible strength and that a deforming fault zone has near-zero thickness (e.g. Cowie and Scholz, 1992).

Natural, shear zones are long, planar features of localized ductile deformation for which plane strain is a first-order satisfactory assumption (Fig. 13). As mentioned earlier, the elastic solutions of fracture mechanics can be mathematically identical to the analytical solutions for viscous deformation (Goodier, 1936). Therefore, the methods developed in fracture mechanics may be extended to viscous shear zones if a finite width is assumed for the shear zone.

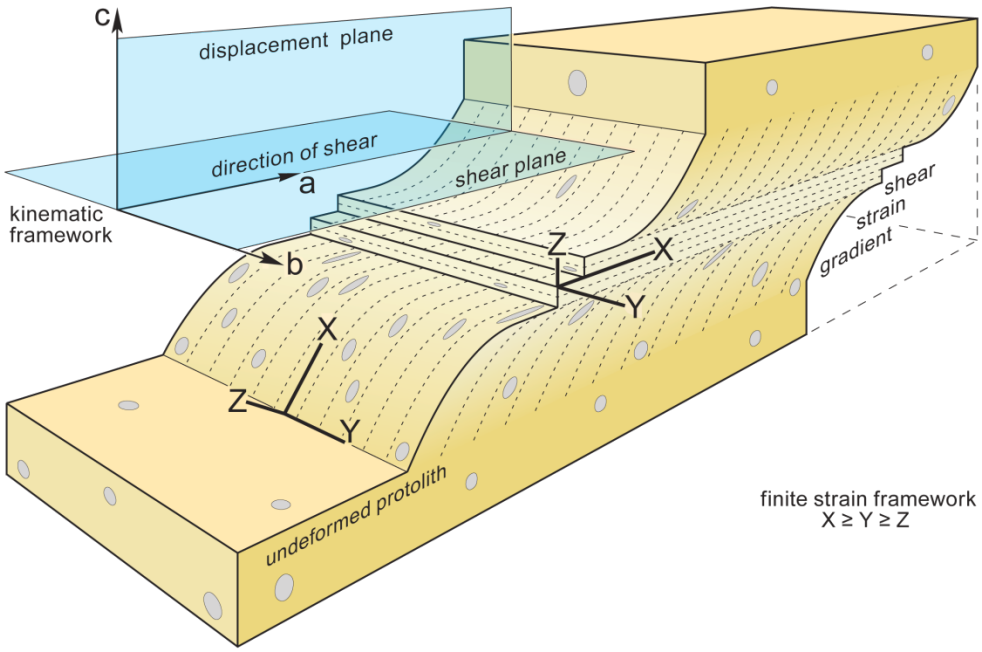

Fig. 13. Unscaled sketch diagram of a natural shear zone and reference frameworks. Small heterogeneities and foliation planes are used as strain markers. Note that in a natural shear zone, no conclusion can be drawn for the exact orientation of the far-field-stress relative to the finite-strain framework. Modified after (Burg, 1999).

Deformation localization involves several types of rheological softening (e.g. Poirier, 1980) so that a shear zone can be treated as elliptical heterogeneity of lower viscosity than the less deformed wall rock. For a weak zone that is one order of magnitude weaker than the surrounding rocks (e.g. Fig. 2), the pressure within the weak zone can reach the order of the far-field stress for $45^{o}<\alpha<90^{o}$. The values of the far-field stress in the lithosphere during shortening are at average 0.1GPa (Schmalholz et al., 2014) and can be locally 0.5-1GPa (e.g. Andersen et al., 2008; Burg and Schmalholz, 2008; Hartz and Podladchikov, 2008). Similar values have actually been measured in experiments simulating the brittle-ductile regime (Hirth and Tullis, 1994). This implies that the overpressure recorded in weak zones at a high angle to compression may be in the order of 1 GPa. In addition, the strong matrix around weak inclusions may undergo pressure perturbations twice as big as the far field shear stress against the inclusion/matrix interface (θ between 50 and 120 in Fig. 5d).

Competent boudins

Viscous heterogeneities are commonly inherited from lithological changes like in the case of competent boudins embedded in a low viscosity matrix (Fig. 14). The effective viscosity for crustal

lithologies during deformation can vary several orders of magnitude, from ca 10^{19} to 10^{25} Pa·s (e.g. Homburg et al., 2010; Sizova et al., 2012). Applying the results displayed in Fig. 3, an effective viscosity contrast of 10 between a strong boudin and a weaker rock will create pressure variations as large as the magnitude of the maximum shear stress. The maximum shear stress is limited by the strength of rocks. Considering the strength of eclogites at temperatures < 1000 ºC (ca. 1GPa; e.g. Moghadam et al., 2010), the pressure in strong inclusions can be up to 1GPa higher than the lithostatic if the inclusion is parallel to the shortening direction. This may explain common geological record of metamorphic pressure higher in mafic/ultramafic boudins than within their surrounding gneiss matrix (e.g. Godard, 2001).

Fig. 14. Boudinage in blueschists, Île de Groix. Location: N 47º37'15.5'', W 03º25'27.0''.

DISCUSSION

Elliptical viscous inclusions were used to analyze the pressure and stress fields caused by elongated bodies or shear zones in the lithosphere. Pressure in a weak inclusion is given by equation 10, which can be further simplified, assuming low viscosity ratios, to:

$$\frac{P^i}{\tau_{ffs}} \cong -\frac{\left(\kappa^2-1\right)}{\kappa^2+1}\cos\left(2\alpha\right) \qquad (13)$$

Pressure in a competent (more viscous) inclusion is approximated with another simplification of

equation 10:

$$\frac{P^i}{\tau_{ffs}} \cong \frac{\left(\frac{\mu^i}{\mu^m}\right)\kappa}{2\left(\frac{\mu^i}{\mu^m}\right)+\kappa}\cos(2\alpha) \qquad (14)$$

The lithostatic load and the far-field tectonic stress have to be taken into account to assess the magnitude of the total pressure within the inclusion. Introducing equation 10 in equation 8, and considering that the far-field mean stress includes also a non-lithostatic component (c.f. Petrini and Podladchikov, 2000) the actual pressure (in Pa) in the inclusion is:

$$P^i_{tot} = \rho g h + \tau_{ffs} + \tau_{ffs}\frac{\left(\frac{\mu^i}{\mu^m}-1\right)(\kappa^2-1)}{2\left(\frac{\mu^i}{\mu^m}\right)\kappa+\kappa^2+1}\cos(2\alpha) \qquad (15)$$

The first term in the right hand side of equation 15 is the pressure contribution from the lithostatic load. The second term is the effect that the far-field tectonic stress has on the mean stress of the matrix. The last term is the pressure caused by the viscosity heterogeneity. If the elliptical heterogeneity is close to the brittle-ductile condition, then the magnitude of τffs is about the lithostatic load ($\rho g h$; Petrini and Podladchikov, 2000). Then, the mean stress experienced by the elliptical heterogeneity is:

$$P^i_{tot} \cong 2\rho g h + \frac{\left(\frac{\mu^i}{\mu^m}-1\right)(\kappa^2-1)}{2\left(\frac{\mu^i}{\mu^m}\right)\kappa+\kappa^2+1}\cos(2\alpha)\rho g h \cong \begin{cases} 2\rho g h - \frac{(\kappa^2-1)}{\kappa^2+1}\cos(2\alpha)\rho g h, & \frac{\mu^i}{\mu^m} \ll 1 \\ 2\rho g h + \frac{\left(\frac{\mu^i}{\mu^m}\right)\kappa}{2\left(\frac{\mu^i}{\mu^m}\right)+\kappa}\cos(2\alpha)\rho g h, & \frac{\mu^i}{\mu^m} \gg 1 \end{cases} \qquad (16)$$

which can be illustrated with a Mohr construction where each contributing pressure is separately visualized (Fig. 15).

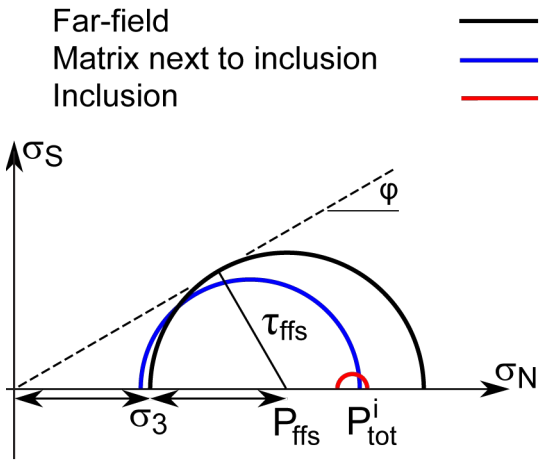

Fig. 15. Mohr diagram showing a hypothetical scenario where a weak inclusion and a strong matrix are close to the brittle-ductile transition. The far-field compressive stress of the matrix is indicated by τ_{ffs}. P_{ffs} is the far-field mean stress during deformation. σ_3 is commonly assumed to be equal to P_{lith} (Eq. 1) in compressional settings. If the angle of internal friction (φ) is taken to be 30º, then P_{ffs} may reach 2ρgh (Petrini and Podladchikov, 2000) and a weak inclusion may have a mean stress larger than 2ρgh.

The Muskhelishvili's method employs the effective-viscosity contrast at the time of the deformation. Therefore, the competence contrast is sufficient to create perturbations in the effective shear stress (τ) and pressure (P) and this does not depend on the specific rheological model as long as viscosity variations exist. This means that variations in pressure are a first-order physical phenomenon related to stress heterogeneities, whatever the rheological model. The spatial pattern of tectonic stress and pressure fields in and out of deforming elliptical inclusions depends in two factors, one being purely geometrical (aspect ratio, inclusion orientation to the far-field stress) and the other being the competence contrast (viscosity ratio).

Geometrical factor

The application of the Kolosov-Muskhelishvili's equations for elliptical viscous heterogeneities under viscous flow predicts that variations in the pressure/stress fields during deformation are functions of viscosity heterogeneities and geometrical factors such as the orientation of the inclusion relative to the far-field stress. The perturbation magnitude amplifies with higher aspect ratios of the inclusion. In this work we used a finite-width inclusion. Natural, elongated inclusions have aspect ratios spanning up to 4 orders of magnitude.

Rheological factor

Pressure variations are proportional to the viscosity ratio between the inclusion and the matrix. The pressure difference ΔP (P^i-P^m) predicted for strong inclusions (the length of abscissa between centers of corresponding Mohr circles, Fig. 3b) increases with the effective shear stress τ (the radius of the Mohr

circle) of this inclusion (for example compare Figs. 3a and b). An apparent paradox is that the pressure difference in weak inclusions is inversely related to the applied effective shear stress τ (see size and location of red inclusion circle in Fig. 2). Pressure variations within weak zones may reach but not overcome the same magnitude as the far-field tectonic stress (black circle in Fig. 2). These variations will thus be limited by the effective shear stress (blue circle radius) that develops in the adjacent strong lithologies.

Time factor

The results presented here concern the instantaneous case. However, both geometrical configuration and viscosity contrast may evolve with time. Bulk strain may reorient any sort of particle with respect to shortening direction (e.g. Ramberg and Ghosh, 1977), thus impelling changes in the effective shear stress and pressure. Such changes can be considerable, yet independent of lithostatic pressure. Consequently, the time evolution of effective shear stress and pressure is important and the question that rises is whether the pressure variations calculated in this work may last sufficiently long to be recorded by the metamorphic phase equilibria. If yes, the fast decompression rates experienced by some metamorphic rocks do not necessarily correspond to changes in depth. In the case of lithospheric shortening, viscous heterogeneities are submitted to the far-field stress for as long as shortening persists. Therefore, crustal regions like the Alpine-Himalayan Belt, which has been under compression for millions of years (e.g. Dewey and Şengör, 1979; Burg, 2012) have sufficient time to record transient pressure variations, especially at lower crustal conditions where the high temperature enhances mineral reactions. Finally, metamorphic reactions may modify the actual physical properties of deforming rocks. For instance, processes such as dehydration, melting or eclogitization significantly change viscosity. Therefore, a small viscosity ratio may amplify with metamorphic reactions, leading to amplification of effective shear stress and pressure variations as well.

CONCLUSIONS

Analytical solutions derived from the Muskhelishvili's method show that the aspect ratio and the orientation of elliptical inclusions are important factors for sharp disturbances in effective shear stress and pressure fields inside and outside viscous inclusions. The analytical solution also suggests that the magnitude of the pressure variations can reach the magnitude of the far-field tectonic stress, which is in the order of 1 GPa for crustal conditions. This result is consequential in the geodynamic interpretation

of metamorphic rocks, in particular as to whether ultra-high and high metamorphic pressures of mafic layers/boudins/nappes are applicable to their entire gneissic matrix. If viscous heterogeneities produce pressure differences, then rapid decompression/exhumation rates that arise from converting metamorphic pressure to depth are disputable.

ACKNOWLEDGMENTS

E.M. acknowledges the Alexander S. Onassis Public Benefit Foundation (F-ZF 053/2009-2010), the ETH Zurich, the ERC starting grant (335577) and the University of Lausanne for financial support. Stefan Schmalholz is acknowledged for allowing us to use the data from the numerical results presented in this study. Marcel Frehner is acknowledged for helpful discussions. Dave May and Taras Gerya are acknowledged for their detailed and constructive criticism that helped in improving the paper. Editorial handling by Evgueni Burov and Laurent Jolivet is appreciated.

REFERENCES

Andersen TB, Mair K, Austrheim H, et al (2008) Stress release in exhumed intermediate and deep earthquakes determined from ultramafic pseudotachylyte. Geology 36:995–998. doi: 10.1130/G25230A.1

Brace WF, Ernst WG, Kallberg RW (1970) An Experimental Study of Tectonic Overpressure in Franciscan Rocks. Geological Society of America Bulletin 81:1325–1338. doi: 10.1130/0016-7606(1970)81[1325:AESOTO]2.0.CO;2

Burg JP (1999) Ductile structures and instabilities: their implication for Variscan tectonics in the Ardennes. Tectonophysics 309:1–25. doi: 10.1016/S0040-1951(99)00129-8

Burg JP (2012) Rhodope: From Mesozoic convergence to Cenozoic extension. Review of petro-structural data in the geochronological frame. Journal of the Virtual Explorer 42:2–44. doi: 10.3809/jvirtex.2011.00270

Burg J-P, Schmalholz SM (2008) Viscous heating allows thrusting to overcome crustal-scale buckling: Numerical investigation with application to the Himalayan syntaxes. Earth and Planetary Science Letters 274:189–203. doi: 10.1016/j.epsl.2008.07.022

Burov E, Jolivet L, Le Pourhiet L, Poliakov A (2001) A thermomechanical model of exhumation of high pressure (HP) and ultra-high pressure (UHP) metamorphic rocks in Alpine-type collision belts. Tectonophysics 342:113–136. doi: 10.1016/S0040-1951(01)00158-5

Clark SP (1961) A redetermination of equilibrium relations between kyanite and sillimanite. American Journal of Science 259:641–650. doi: 10.2475/ajs.259.9.641

Cowie PA, Scholz CH (1992) Physical explanation for the displacement-length relationship of faults using a post-yield fracture mechanics model. Journal of Structural Geology 14:1133–1148. doi: 10.1016/0191-8141(92)90065-5

Dahlen FA (1992) Metamorphism of nonhydrostatically stressed rocks. American Journal of Science 292:184–198. doi: 10.2475/ajs.292.3.184

Dewey JF, Şengör AMC (1979) Aegean and surrounding regions: Complex multiplate and continuum tectonics in a convergent zone. Geological Society of America Bulletin 90:84–92. doi: 10.1130/0016-7606(1979)90<84:AASRCM>2.0.CO;2
Godard G (2001) Eclogites and their geodynamic interpretation: a history. Journal of Geodynamics 32:165–203. doi: 10.1016/S0264-3707(01)00020-5
Goodier JN (1936) Slow viscous flow and elastic deformation. Philosophical Magazine Series 7 22:678–681. doi: 10.1080/14786443608561718
Griffith AA (1921) The Phenomena of Rupture and Flow in Solids. Philosophical Transactions of the Royal Society of London Series A, 221:163–198. doi: 10.1098/rsta.1921.0006
Hartz EH, Podladchikov YY (2008) Toasting the jelly sandwich: The effect of shear heating on lithospheric geotherms and strength. Geology 36:331–334. doi: 10.1130/G24424A.1
Hirth G, Tullis J (1994) The brittle-plastic transition in experimentally deformed quartz aggregates. Journal of Geophysical Research: Solid Earth 99:11731–11747. doi: 10.1029/93JB02873
Homburg JM, Hirth G, Kelemen PB (2010) Investigation of the strength contrast at the Moho: A case study from the Oman Ophiolite. Geology 38:679–682. doi: 10.1130/G30880.1
Inglis CE (1913) Stresses in a plate due to the presence of cracks and sharp corners. Trans Inst Naval Architects 55:219–230.
Irwin GR (1957) Analysis of stresses and strains near the end of a crack traversing a plate. Journal of Applied Mechanics 24:361–364.
Jamieson JC (1963) Possible occurence of exceedingly high pressures in geological meterials. Geological Society of America Bulletin 74:1067–1070. doi: 10.1130/0016-7606(1963)74[1067:POOEHP]2.0.CO;2
Jolivet L, Faccenna C, Goffé B, et al (2003) Subduction tectonics and exhumation of high-pressure metamorphic rocks in the Mediterranean orogens. American Journal of Science 303:353–409. doi: 10.2475/ajs.303.5.353
Kolosov GV (1909) On the application of the theory of functions of a complex variable to plane problems of the mathematical theory of elasticity, Dissertation. St. Petersburg
Lambe TW, Whitman RV (1968) Soil Mechanics. John Wiley & Sons, Inc.
Llana-Fúnez S, Wheeler J, Faulkner DR (2012) Metamorphic reaction rate controlled by fluid pressure not confining pressure: implications of dehydration experiments with gypsum. Contrib Mineral Petrol 164:69–79. doi: 10.1007/s00410-012-0726-8
Mancktelow NS (2008) Tectonic pressure: Theoretical concepts and modelled examples. Lithos 103:149–177. doi: 10.1016/j.lithos.2007.09.013
Means WD (1976) Stress and Strain: Basic Concepts of Continuum Mechanics for Geologists,. Springer
Moghadam RH, Trepmann CA, Stöckhert B, Renner J (2010) Rheology of Synthetic Omphacite Aggregates at High Pressure and High Temperature. Journal of Petrology 51:921–945. doi: 10.1093/petrology/egq006
Muskhelishvili NI (1953) Some Basic Problems of the Mathematical Theory of Elasticity. Noordhoff, Groningen
Nadai A (1950) Theory of flow and fracture of solids, 2nd edn. McGraw-Hill
Paterson MS (1973) Nonhydrostatic Thermodynamics and Its Geologic Applications. Reviews of Geophysics and Space Physics 11:355–389.
Perchuk LL (1991) Derivation of a thermodynamically consistent set of geothermometers and geobarometers for metamorphic and magmatic rocks. In: Perchuk LL (ed) Progress in metamorphic and magmatic petrology, a memorial volume in honor of D.S. Korzhinskiy.

Cambridge University Press, pp 93–111
Petrini K, Podladchikov Y (2000) Lithospheric pressure–depth relationship in compressive regions of thickened crust. Journal of Metamorphic Geology 18:67–77. doi: 10.1046/j.1525-1314.2000.00240.x
Poirier JP (1980) Shear localization and shear instability in materials in the ductile field. Journal of Structural Geology 2:135–142. doi: 10.1016/0191-8141(80)90043-7
Pollard DD, Fletcher RC (2005) Fundamentals of Structural Geology. Cambridge University Press
Ramberg H, Ghosh SK (1977) Rotation and strain of linear and planar structures in three-dimensional progressive deformation. Tectonophysics 40:309–337. doi: 10.1016/0040-1951(77)90071-3
Schmalholz SM, Medvedev S, Lechmann SM, Podladchikov Y (2014) Relationship between tectonic overpressure, deviatoric stress, driving force, isostasy and gravitational potential energy. Geophysical Journal International 197:680–696. doi: 10.1093/gji/ggu040
Schmalholz SM, Podladchikov YY (2013) Tectonic overpressure in weak crustal-scale shear zones and implications for the exhumation of high-pressure rocks. Geophysical Research Letters 40:1984–1988. doi: 10.1002/grl.50417
Schmid DW, Podladchikov YY (2003) Analytical solutions for deformable elliptical inclusions in general shear. Geophysical Journal International 155:269–288. doi: 10.1046/j.1365-246X.2003.02042.x
Sizova E, Gerya T, Brown M (2012) Exhumation mechanisms of melt-bearing ultrahigh pressure crustal rocks during collision of spontaneously moving plates. Journal of Metamorphic Geology 30:927–955. doi: 10.1111/j.1525-1314.2012.01004.x
Timoshenko S, Goodier JN (1951) Theory of Elasticity, 2nd edn. McGraw-Hill